Parabolized Navier-Stokes Analysis of Ducted Supersonic Combustion Problems

N. Sinha* and S. M. Dash†
Science Applications International Corporation, Princeton, New Jersey

The extension of a recently developed implicit/explicit approach to analyzing two-dimensional ducted supersonic mixing problems with finite-rate chemistry is presented. The hybrid approach combines a fully implicit parabolic mixing algorithm, an explicit viscous-characteristic-based wave-solver algorithm, and a linearized implicit chemical kinetic solution algorithm. The resultant model provides spatial marching solutions of the parabolized Navier-Stokes (PNS) equations for supersonic combustion problems. Specialized procedures are incorporated to deal with the near-wall sublayer. A parabolic option is available that can be utilized in the direct or inverse mode for design applications. The ability of the model to treat shock waves and wave/mixing layer interactions is assessed via comparisons of predictions with those of well-established, explicit shock-capturing Euler (SCIPPY) and PNS (SCIPVIS) models. Applications to several supersonic combustion flowfield problems are presented that exhibit overall capabilities.

Nomenclature

a,b = mapping parameters
$F^{\pm}$ = diffusive/chemical kinetic source term
h_i = static enthalpy of the ith species
H = total enthalpy
k = turbulent kinetic energy
M = Mach number
m_i = molecular weight of the ith species
$P,\tilde{P}$ = pressure and ℓnP
P = turbulent production term, $=\tilde{\mu}[\partial u/\partial y]^2$
R_0 = universal gas constant
r = radial distance from flow axis, $=r_b(x)+y\cos\alpha_B(x)$
T = temperature
u,v = velocity components in x,y coordinate directions
W = mixture molecular weight
x,y = streamwise and boundary-layer transverse coordinates
α_B = inclination of body surface with respect to flow axis
α_i = mass fraction of ith chemical species
γ = specific heat ratio
ϵ = turbulent dissipation rate
μ = Mach angle
$\tilde{\mu}$ = effective viscosity
ξ,η = mapped coordinates
ρ = density
$\tilde{\sigma}$ = effective viscosity/Prandtl number, $=\mu_l/P_{r_l}+\mu_t/P_{r_t}$
$\tilde{\sigma}_{k,\epsilon}$ = effective viscosity/Prandtl number for turbulence model equations
ϕ = angle of mapped coordinate line
$\dot{\omega}_i$ = chemical kinetic production term of ith species

Presented as Paper 86-0004 at the AIAA 24th Aerospace Sciences Meeting, Reno, NV, Jan. 1986; received July 23, 1987.

*Technical Director, Propulsion Gas Dynamics Division. Member AIAA.
†Chief Scientist, Fluid and Material Sciences Operation. Member AIAA.

Introduction

WHILE parabolized Navier-Stokes (PNS) methodology is usually associated with models first developed in the 1970s to analyze supersonic external aerodynamic problems, the first PNS models were developed in the early 1960s for the analysis of supersonic combustion flowfields. This body of work, entitled viscous characteristics (VSCH), was pioneered by Ferri[1,2] with explicit-based numerical techniques developed by Morretti,[3] Edelman,[4] and Dash[5,6] for treating coupled wave/mixing/chemical kinetic processes. The detailed treatment of near-wall regions was first provided for by use of an inner, implicit parabolic solver interactively coupled to the outer explicit VSCH solver at the boundary-layer sonic line.[7]

The VSCH approach involves a *splitting* of the PNS solution, at each integration step, into two coupled solutions, namely:

1) A *parabolic mixing solution*, providing solutions of the streamwise momentum, energy, species, and turbulence model equations, with the pressure field stipulated.

2) A *hyperbolic pressure/wave-field solution*, providing solutions of the continuity and normal momentum equations, cast into viscous-characteristic form, yielding the pressure field and flow angles, with viscous stress/transport and chemical kinetic terms stipulated.

Earlier VSCH approaches were fully explicit and utilized characteristic networks to determine the wave field. Such models could not capture embedded shock waves, and the coding logic entailed to handle various flow situations with fitted shock waves was extremely complex.

An upgrade to splitting-based PNS methodology was made by Spalding and co-workers in the mid-1970s (see, e.g., Refs. 8 and 9) by utilizing fully implicit numerics. As in the VSCH approach, the solution was split into parabolic and pressure-solver components. The parabolic component utilized standard implicit methodology. A continuity-based pressure correction equation was used to determine the pressure field with the parabolic and pressure correction equations iterated upon until a converged solution was obtained. Whereas the implicit numerics in the Spalding pressure-split approach represented a significant upgrade to the explicit numerics utilized in earlier VSCH approaches, the iterations required were time-consuming, and waves were represented in a highly smeared fashion.

The hybrid implicit/explicit approach[10] utilized in the subject duct flow model represents a unification of the better

features of VSCH and Spalding-based PNS methodology. This approach combines a fully implicit parabolic mixing solver with an explicit, viscous-characteristic-based wave solver. The wave solver casts the characteristic differential equations into an upwind finite-difference form that is shown to have good shock-capturing capabilities. The duct flow model incorporates methodology originally developed for freejet and wall-jet models, which includes:

1) A hybrid k-ϵ/Van Driest (near-wall) turbulence model, validated for wall-jet/slot-injection problems at lower speeds.[11]

2) A well-established, implicit, chemical kinetics solver[12] (which serves as a component of numerous JANNAF standard codes for rocket propulsion applications), whose coupling with the implicit parabolic mixing solver for free shear flows is described in Ref. 13.

3) An upwind, characteristic-based wave solver whose preliminary description was given in Ref. 10.

The new capabilities described in this article derive from the unification and extension of the parabolic mixing and above methodology into a model for ducted, turbulent reacting flows. The extensions have involved primarily the development of various, specialized procedures to facilitate obtaining a coupled solution of combustion kinetics, turbulent mixing, and wave processes in a ducted environment. The model provides for the treatment of moderate-strength embedded shocks (due to underexpanded or angled fuel jets and/or incoming shock waves from the upstream flow) and contains pressure-gradient-based artificial diffusion terms for strong shock stabilization and entropy production in inviscid regions. The treatment of small, embedded zones of subsonic flow is handled by utilization of sublayer-type approximation. Special attention has been given to grid-related issues for dealing with the disparate scales of the problem. These include utilizing different radial grid spacing for wave and mixing processes (which is facilitated by the splitting approach taken) and incorporating adaptive step-size controls keyed to the time scales of the kinetics.

Governing Equations

Mean Flow Equations

The two-dimensional (planar, $J=0$; cylindrical, $J=1$) ducted mixing layer mean flow and turbulence model equations utilized for a generalized, multicomponent gas mixture flows are listed as follows.

Continuity:

$$\frac{\partial}{\partial x}(\rho u r^J)+\frac{\partial}{\partial y}(\rho v r^J)=0 \tag{1}$$

Axial momentum:

$$\rho u\frac{\partial u}{\partial x}+\rho v\frac{\partial u}{\partial y}+\frac{\partial P}{\partial x}=\frac{1}{r^J}\frac{\partial}{\partial y}\left[r^J\tilde{\mu}\frac{\partial u}{\partial y}\right]=F_u \tag{2}$$

Radial momentum:

$$\rho u\frac{\partial v}{\partial x}+\rho v\frac{\partial v}{\partial y}+\frac{\partial P}{\partial y}=\frac{1}{r^J}\frac{\partial}{\partial y}\left[\frac{4}{3}r^J\tilde{\mu}\frac{\partial v}{\partial y}\right]-\frac{2}{3}\frac{\partial(\rho k)}{\partial y}-\frac{J}{r}\left[\frac{2}{3}v\frac{\partial\tilde{\mu}}{\partial y}+\frac{4}{3}\frac{\tilde{\mu}v}{r}\right]=F_v \tag{3}$$

Energy:

$$\rho u\frac{\partial H}{\partial x}+\rho v\frac{\partial H}{\partial y}=\frac{1}{r^J}\frac{\partial}{\partial y}\left[r^J\tilde{\sigma}\frac{\partial H}{\partial y}\right]+\frac{1}{r^J}\frac{\partial}{\partial y}\left[r^J(\tilde{\mu}-\tilde{\sigma})\frac{\partial}{\partial y}\left(\frac{u^2}{2}\right)\right]=F_H \tag{4}$$

Species continuity:

$$\rho u\frac{\partial\alpha_i}{\partial x}+\rho v\frac{\partial\alpha_i}{\partial y}=\frac{1}{r^J}\frac{\partial}{\partial y}\left[r^J\tilde{\sigma}\frac{\partial\alpha_i}{\partial y}\right]+\dot{\omega}_i=F_{\alpha_i} \tag{5}$$

Turbulent kinetic energy:

$$\rho u\frac{\partial k}{\partial x}+\rho v\frac{\partial k}{\partial y}=\frac{1}{r^J}\left[r^J\frac{\partial}{\partial y}\left(\tilde{\sigma}_k\frac{\partial k}{\partial y}\right)\right]+P-\rho\epsilon \tag{6}$$

Turbulent dissipation rate:

$$\rho u\frac{\partial\epsilon}{\partial x}+\rho v\frac{\partial\epsilon}{\partial y}=\frac{1}{r^J}\left[r^J\frac{\partial}{\partial y}\left(\tilde{\sigma}_\epsilon\frac{\partial\epsilon}{\partial y}\right)\right]+\frac{\epsilon}{k}(C_1P-C_2\rho\epsilon) \tag{7}$$

In the energy and species continuity equations, the transport of mass and energy is taken to be the same (Lewis number of unity is assumed) and, hence, the Prandtl and Schmidt numbers are equivalent. These equations are supplemented by the equation of state:

$$P=\rho R_0 T\Sigma\alpha_i/m_i \tag{8}$$

and the relation between temperature and static enthalpy:

$$h=\Sigma\alpha_i h_i(T) \tag{9}$$

Curve fits for species enthalpy, $h_i(T)$, and Gibbs free energy, $g_i(T)$ (utilized in the chemical kinetic solution), are based on those of Gordon and McBride.[14] Curve fits for laminar transport data (viscosity, thermal conductivity, Prandtl number) for the various species are based on the data of Svehla.[15] Standard binary diffusion concepts are utilized in defining laminar transport coefficients.

Mapped Parabolic Equations

The governing equations are integrated in mapped rectangular coordinates defined by the transformation:

$$\xi=x$$

$$\eta=\frac{y-y_L(x)}{y_U(x)-y_L(x)} \tag{10}$$

where $y_L(x)$ and $y_U(x)$ are the lower and upper boundaries of the computational domain. The parabolic system of equations (axial momentum, energy, species continuity, and turbulence model equations) in these mapped coordinates are cast in the vectorized form

$$\rho u\frac{\partial\bar{f}}{\partial\xi}+b\rho\tilde{v}\frac{\partial\bar{f}}{\partial\eta}=\frac{b^2}{r^J}\frac{\partial}{\partial\eta}\left[r^J\tilde{\sigma}_f\frac{\partial\bar{f}}{\partial\eta}\right]+\bar{g}_f \tag{11}$$

where $\bar{f}=[u,H,\alpha_i,k,\epsilon]^T$, $\tilde{v}=v-au/b$, $\tilde{\sigma}_f=[\tilde{\mu},\tilde{\sigma},\tilde{\sigma},\tilde{\sigma}_k,\tilde{\sigma}_\epsilon]$, and a and b are the mapping parameters:

$$a(\xi,\eta)=[(1-\eta)y_L'+\eta y_U']/(y_U-y_L)$$

$$b(\xi)=1/(y_U-y_L) \tag{12}$$

Wave-Solver Equations

By the manipulations discussed in Refs. 10 and 16, the continuity and normal momentum equations can be cast into characteristic form with the viscous stress/transport and chemical kinetic terms [the right-hand side terms of Eqs.

(2-5), designated F_u, F_v, F_H, F_{α_i}, respectively] treated as source terms in performing these manipulations. Along the characteristic directions $\lambda^{\pm}$, given by

$$\frac{dy}{dx} = \tan(\theta \pm \mu) \tag{13}$$

the viscous-characteristic compatibility relations take the form

$$\frac{\sin\mu \cos\mu}{\gamma} \frac{d\tilde{P}}{d\lambda^{\pm}} \pm \frac{d\theta}{d\lambda^{\pm}} = F^{\pm} \tag{14}$$

where $\tilde{P} = \ell n P$ and the source term $F^{\pm}$ is given by

$$F^{\pm} = \frac{-J}{r} \sin\theta \sin\mu + \frac{(\gamma-1)\sin\mu}{\gamma PQ} \times \left\{ F_H + \sum_i \left[\left(\frac{C_P WT}{m_i} - h_i \right) F_{\alpha_i} \right] \right\} - \frac{F_u}{\gamma PM^2} \times \{ [1+(\gamma-1)M^2] \sin\mu \cos\theta \pm \cos\mu \sin\theta \} - \frac{F_v}{\gamma PM^2} \{ [1+(\gamma-1)M^2] \sin\mu \sin\theta \pm \cos\mu \cos\theta \} \tag{15}$$

Referring to Fig. 1, the characteristic compatibility relations comprising total differentials along $\lambda^{\pm}$ are cast into partial differential expressions along the mapped coordinate directions ξ and η, using the relation

$$\left. \frac{d}{dx} \right|_{\lambda^{\pm}} = \frac{\partial}{\partial \xi} + \lambda^{\pm} \frac{\partial}{\partial \eta} \tag{16}$$

where

$$\lambda^{\pm} = \tan(\theta \pm \mu) - \tan\phi \tag{17}$$

and ϕ denotes the angle of the mapped coordinate line $\eta = \text{const}$, with respect to the x direction. Then, the characteristic compatibility relations can be written in the following partial differential form

$$C\left[\frac{\partial \tilde{P}}{\partial \xi} + \lambda^{\pm} b \frac{\partial \tilde{P}}{\partial \eta} \right] \pm \left[\frac{\partial \theta}{\partial \xi} + \lambda^{\pm} b \frac{\partial \theta}{\partial \eta} \right] = \tilde{F}^{\pm} \tag{18}$$

where $C = (\sin\mu \cos\mu)/\gamma$ and $\tilde{F} = F/\cos(\theta \pm \mu)$. Equation (18) comprises two independent relations for $\tilde{P}$ and θ to be evaluated at each grid point.

Hybrid Turbulence Model and Near-Wall Coupling

The hybrid turbulence model employed is described in Ref. 11 and utilizes a standard high Reynolds number k-ϵ model coupled to a near-wall damped Van Driest model at $y^+ = 50$. Coupling between the Van Driest near-wall model and the outer region k-ϵ model is based on matching the two turbulent viscosities and stipulating that the turbulence (at $y^+ = 50$) is in a state of equilibrium (turbulent production equals turbulent dissipation). Stipulating these coupling relations serves to provide near-wall boundary conditions for the k-ϵ turbulence model dependent variables, k and ϵ, at the grid point nearest to $y^+ = 50$ at each axial station. The coupling approach taken is analogous to that of Arora et al., which is described in detail in Ref. 17. The basic k-ϵ model constants utilized[11] are as follows: $C_1 = 1.43$, $C_2 = 1.92$, $C_\mu = 0.09$, $\tilde{\sigma}_k = \tilde{\mu}$, $\sigma_\epsilon = \tilde{\mu}/1.3$. The k-ϵ turbulent viscosity is given by the relation

$$\mu_t = C_\mu \rho k^2/\epsilon \tag{19}$$

Chemical Kinetics

The evaluation of the chemical production term for the ith species equation $\dot{\omega}_i$ is based on the linearized implicit approach first formulated by Tyson and Kliegel[18] and described in the text by Zucrow and Hoffman.[19] The first application of this approach to a generalized multicomponent problem was described in Ref. 12. The chemical kinetic package of Ref. 12 serves as the basis for many current JANNAF standardized codes for rocket nozzles and plumes and forms the basis for the chemical kinetic package in the subject duct flow code. The chemical kinetic production term for α_i can be expressed in the form

$$\dot{\omega}_i(T,\rho,\alpha_j) = \sum_{j=1}^{N_i} k_{f_j} \left[a_j \frac{\alpha_m}{m_m} \frac{\alpha_n}{m_n} - \frac{b_j}{K_{P_j}} \left(\frac{\alpha_1}{m_1} \frac{\alpha_m}{m_m} \frac{\alpha_n}{m_n} \right) \right] \tag{20}$$

for generalized chemical systems described by a total of NR two- and three-body reactions (see Refs. 12 and 16). The summation for the ith species equation is performed only over those reactions ($j = 1,2,\ldots,N_i$) in which the ith species is involved. The coefficients a_j and b_j are functions of ρ, T, and m. The detailed "bookkeeping" to establish $\dot{\omega}_i$ in the form given by Eq. (20) is described in Ref. 12. In formulating Eq. (20), forward reaction rates are evaluated with the reaction rate coefficient k_f whereas backward reaction rates are expressed in terms of k_f and the equilibrium constant K_P (namely, $k_b = k_f/K_p$), whose evaluation requires curve fits of Gibbs free energy.[14]

Parabolic Computational Techniques

Generalized Implicit Algorithm

The mapped, vectorized parabolic system of equations (Eq. 11) is solved using conventional finite-difference methodology. The convective terms are differenced using upwind, central, or hybrid difference approximations; the dif-

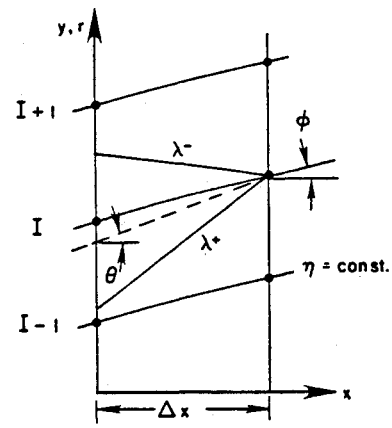

CARTESIAN/CYLINDRICAL SYSTEM

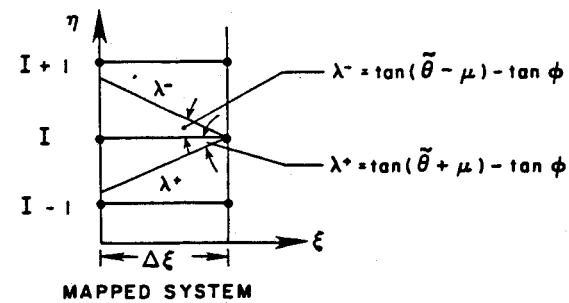

MAPPED SYSTEM

Fig. 1 Characteristic nomenclature in Cartesian/cylindrical coordinates and in mapped ξ,η coordinates.

fusive terms are represented by central differences. Differences are evaluated at $\xi+\Delta\xi$ (fully implicit) or averaged over the integration step (Crank-Nicholson). The grid spacing in the radial direction is arbitrary and can be user-defined (e.g., fixed values of $\eta(I)$ are input where I is the radial grid point) or defined via standard grid-clustering expressions.[20] The individual mean flow and turbulence model equations are solved in an uncoupled manner with the coefficients lagged and the source terms treated explicitly. This uncoupled approach has proved efficient for both diffusion-controlled combustion problems, where the axial integration step is limited by kinetic requirements and the kinetic and diffusive grid scales must be the same, and kinetic-controlled problems that permit kinetic step-splitting.

The numerical algorithm for integrating the dependent variable f at grid point I (in marching from ξ to $\xi+\Delta\xi$) takes the standard tridiagonal form

$$A_I f_{I-1}+B_I f_I+C_I f_{I+1}=D_I \tag{21}$$

where the coefficients A-D are evaluated, based on properties at ξ. The code provides for iterating the integration (with the coefficients A-D averaged across the step) and has the step size $\Delta\xi$ keyed to the axial flow gradients [a feedback system is utilized based on user-specified allowable changes in key dependent variables (see Ref. 16 for details)]. Equation (21) is evaluated using a standard tridiagonal inversion procedure (see Ref. 16 for complete details).

Boundary and Initial Conditions

The duct code operates parabolically with lower and upper boundaries that can be any combination of geometric surfaces, symmetry planes, or mixer layer edges. This latter option uses an adaptive boundary growth rule formulation keyed to edge gradients[11] and permits operating in a boundary-layer or wall jet mode, as well as in a free shear layer mode. The wall boundary conditions permit the stipulation of both no-slip and slip options with the conditions

$$u=0, \quad v=0, \quad \frac{\partial H}{\partial y}=0 \text{ or } T=T_W(x), \text{ and } \quad \frac{\partial \alpha_i}{\partial y}=0$$

being those typically used at noncatalytic combustor walls with no surface transpiration.

The initial conditions for a parabolic combustor problem with tangential fuel injection typically comprise stipulation of profiles of the axial velocity, temperature, and species mass or mole fractions. Turbulence parameters k and ϵ can be stipulated if available. As a default, the code determines tubulence parameters by evaluating the mixing length scale variation across the duct (with near-wall variations, including those at splitter plates, evaluated using the Escudier formulation[21] as described in the text of Launder and Spalding[22]) and assuming the turbulence (described by a mixing length model) to be in a state of equilibrium.[16] The initial radial velocity profile cannot be "mathematically" stipulated in a purely parabolic problem and is obtained by iterating between the parabolic integration and the integration of the continuity equation at the initial station (or by underrelaxing from a prescribed initial distribution over several integration steps in this manner).

Chemical Kinetic/Fluid Dynamic Coupling

The chemical kinetic solution in the duct code is based on the linearized implicit approach of Tyson and Kliegel,[18,19] utilizing an upgraded version of the chemical kinetic package described in Ref. 12. Both the parabolic fluid dynamic solutions and the chemical kinetic solution are fully implicit. The *coupled* implicit solution of the fluid dynamic/chemical kinetic problem would require the inversion of a complex system of matrices [i.e., at each grid point, the various chemical species are related to each other via the implicit chemical formulation and to the same species at adjacent grid points via the implicit fluid dynamic alogorithm of Eq. (21)]. To avoid the complexities of inverting an $NS\times NS$ block tridiagonal matrix (where NS represents the total number of species), the fluid dynamic and chemical kinetic solutions are uncoupled in performing the step-size integration. The same chemical/fluid dynamic integration step is generally utilized for both solutions, although the chemical step can be split into several steps for kinetic-controlled problems with rapid/stiff kinetic processes, or for minor species (e.g., ionized species) not affecting the mixture thermodynamics.

The species continuity equation solution is uncoupled by first evaluating the "effective" chemical source term in the integration step, ξ to $\xi+\Delta\xi$, based on values of α_i, T, and ρ at ξ. This involves first integrating the relation

$$\rho\frac{d\alpha_i}{dt}=\dot{\omega}_i(\alpha_1,\alpha_2,\ldots\alpha_N,\rho,T) \tag{22}$$

in a fully implicit fashion (i.e., the α_i are evaluated at $t+\Delta t$). The chemical time step Δt, used to integrate Eq. (22), is set equal to the local fluid dynamic time step if no kinetic step-splitting is employed, where step-splitting entails dividing the fluid dynamic step Δt into a number of fractional chemical kinetic time steps. The fluid dynamic time to traverse a grid interval is

$$\Delta t=\left(\frac{u}{\Delta\xi}+b\frac{\tilde{v}}{\Delta\eta}\right)^{-1} \tag{23}$$

The solution procedure employed involves a chemical source term linearization[12] whereby the nonlinear species products at $t+\Delta t$ of $\dot{\omega}_i$ [Eq. (20)] are expressed by the following linear relations below (terms with $\tilde{\alpha}$ are evaluated at $t+\Delta t$; those without are evaluated at t):

$$\tilde{\alpha}_m\tilde{\alpha}_n=\tilde{\alpha}_m\alpha_n+\alpha_m\tilde{\alpha}_n-\alpha_m\alpha_n \tag{24a}$$

$$\tilde{\alpha}_1\tilde{\alpha}_m\tilde{\alpha}_n=\tilde{\alpha}_1\alpha_m\alpha_n+\alpha_1\tilde{\alpha}_m\alpha_n+\alpha_1\alpha_m\tilde{\alpha}_n-2\alpha_1\alpha_m\alpha_n \tag{24b}$$

Then, with k_f, K_p, a_j, and b_j of Eq. (20) evaluated at t, the integration of Eq. (22) at *each* grid point I takes the form

$$A_{ij}\frac{\tilde{\alpha}_j}{m_j}+B_j=0 \tag{25}$$

whose solution for $\tilde{\alpha}_i=\alpha_i(t+\Delta t)$ requires the inversion of an $NS\times NS$ matrix. Solving Eq. (25) then yields the "effective" chemical source term $\dot{\omega}_i(I)$ at grid point I (centered about the integration step) via the relation

$$\dot{\omega}_i(I)=\rho[\alpha_i(I,t+\Delta t)-\alpha_i(I,t)]/\Delta t \tag{26}$$

The species continuity equation [Eq. (5)] is then integrated from ξ to $\xi+\Delta\xi$ in a fully implicit manner with the chemical production term $\dot{\omega}_i(I)$ stipulated as a source term along each grid line, $\eta_I=$ const. If ρ and T change significantly, the process can be iterated upon utilizing values of ρ and T centered across the integration step. In practice, no iterations are employed with the step $\Delta\xi$ adaptively varied to keep ρ and T variations to within prescribed tolerances.

Direct and Inverse Parabolic Solution

In the parabolic mode for ducted flows, the wall geometry (direct mode) or axial pressure variation (inverse mode) is prescribed. Pressure is assumed to vary only in the axial direction, and the normal momentum equation is discarded.

The radial velocity distribution is obtained from a streamfunction inversion of the continuity equation, centered at $\xi+\Delta\xi/2$ and performed after the parabolic step is taken. In the direct mode, the pressure variation in the integration step is obtained in a noniterative manner, with an iterative upgrade provided if values of the correction parameters exceed default values.[16] Integration of the mean flow equations with the pressure projected from the gradient at the previous step leads to an error ψ' in the mass flux at $\xi+\Delta\xi$, which is related to the error in pressure via the relation[16]

$$\psi' = P' \int_{r_L}^{r_U} \left(\frac{\rho u}{\gamma P} - \frac{1}{u} \right) r^J dr \tag{27}$$

In formulating Eq. (27), densities are locally corrected via the perturbation relation $\rho' = P'\rho/(\gamma P)$ (obtained from the energy equation) while velocities are corrected via the perturbation relation $u' = P'/(\rho u)$ (obtained from the axial momentum equation). In the near-wall region, the velocity correction relation is destabilizing (since it does not include the viscous term variation) and is replaced by the following implicit correction equation for u':

$$\rho u \frac{\partial u'}{\partial x} = \frac{1}{r^J} \frac{\partial}{\partial y} \left[\left(r^J \tilde{\mu} \frac{\partial u'}{\partial y} \right) \right] - \frac{\partial P'}{\partial x} \tag{28}$$

Since the near-wall region perturbations have negligible influence on overall mass flux, the correction P' of Eq. (27) remains unaffected owing to the usage of the above near-wall velocity correction.

For design purposes, an inverse parabolic option is available whereby the axial duct pressure variation is prescribed and the duct wall variations are obtained corresponding to the imposed pressure variation. With this option, one wall can be fixed and the other varied, or both can be varied using prescribed weighting factors (that is to say, each wall can provide half the area change, etc.). In marching from ξ to $\xi+\Delta\xi$, the duct area gradient dA/dx is assumed to be that from the previous step. Since the pressure is prescribed, correcting the error in mass flux simply involves modifying the assumed area variation. This can be performed iteratively or noniteratively. The noniterative procedure involves accepting the assumed area variation and correcting the pressure as in the direct approach. In order to compensate for the pressure deviation P' from the prescribed duct pressure, the duct area gradient dA/dx is increased/decreased over the next integration step in accordance with the pressure deviation. This noniterative, self-correcting approach works quite well where flow variations are smooth, but the iterative approach must be used in regions of very rapid combustion.

Parabolized Navier-Stokes Computational Techniques

Explicit Hyperbolic Integration of Pressure/Wave-Solver Equations

The characteristic-based wave-solver relations [Eq. (18)] are cast into finite-difference form by evaluating the streamwise derivative $\partial/\partial\xi$ using a standard two-point difference and evaluating the $\partial/\partial\eta$ derivatives using an *upwind* two-point difference at station ξ, which corresponds to the appropriate characteristic direction [λ^+ characteristics employ backward $(I,I-1)$ differences; λ^- characteristics employ forward $(I,I+1)$ differences]. With the manipulations described in Refs. 10 and 16, a pressure solver finite-difference relation of the form listed below is obtained:

$$\tilde{P}_I(\xi+\Delta\xi) = a_1\tilde{P}_{I+1} + a_2\tilde{P}_I + a_3\tilde{P}_{I-1} + a_4\theta_{I+1} + a_5\theta_I + a_6\theta_{I-1} + \tilde{F}_I \tag{29}$$

The coefficients a_i are combinations of the $C^\pm$ and $\lambda^\pm$ terms of Eq. (18) and are evaluated along the *actual* characteristics. The pressures and flow angles on the right-hand side of Eq. (29) are all evaluated at ξ. The diffusive/chemical kinetic terms contained in the source term $\tilde{F}$ [namely, F_u, F_v, F_H, and F_{α_j} components of Eq. (15)] are evaluated at the grid point I, while the coefficients of these terms are evaluated along the characteristics (see Ref. 16 for details).

Coupled Implicit (Parabolic)/Explicit (Hyperbolic) Solution Procedure in Supersonic Regions

The coupled parabolic/hyperbolic solution is performed in the following three-step sequence:

1) Prediction of pressure field at $\xi+\Delta\xi$ solving Eq. (29) using coefficients evaluated at ξ at characteristic intersection points, and diffusive/kinetic source terms evaluated at ξ at grid points I.

2) Solution of parabolic system of equations [Eq. (11)] yielding f at $\xi+\Delta\xi$ via tridiagonal inversion of Eq. (21). Pressure gradients "prescribed" in accordance with wave-field solution of step 1.

3) Correction of wave field at $\xi+\Delta\xi$ using coefficients averaged along characteristics, whose modified slope yields revised values at ξ also, and values of diffusive/kinetic source terms evaluated at $\xi+\Delta\xi$ if the parabolic algorithm of step 2 is either fully implicit or if a Crank-Nicholson parabolic procedure is utilized, averaged across the integration step.

Near-Wall Subsonic/Supersonic Coupling

The near-wall subsonic/supersonic coupling utilized[10] (Fig. 2) employs a lagged interactive predictor-corrector procedure that imposes the pressure gradient prevailing just outside the sonic line throughout the subsonic region. The imposed pressure gradient, at the predictor level, assumes the flow angle at the near-sonic matching point to equal the local wall angle plus the flow angle relative to the wall prevailing at the previous step, which represents the lagged displacement-thickness effect of the subsonic layer. The actual flow angle is determined from the continuity equation after the parabolic integration, and the wave field is corrected for this angle change in the corrector step of the wave-solver sequence. This approach serves to "uncouple" locally the prediction of the streamwise pressure gradient in the subsonic region from the continuity-based pressure-streamtube divergence/contraction balance. It eliminates destabilizing elliptic (upstream-influence) effects in marching from ξ to $\xi+\Delta\xi$ but still accounts for the strong viscous interactions due to the displacement effect of the subsonic layer. Complete details are given in Refs. 10 and 16 with validation of

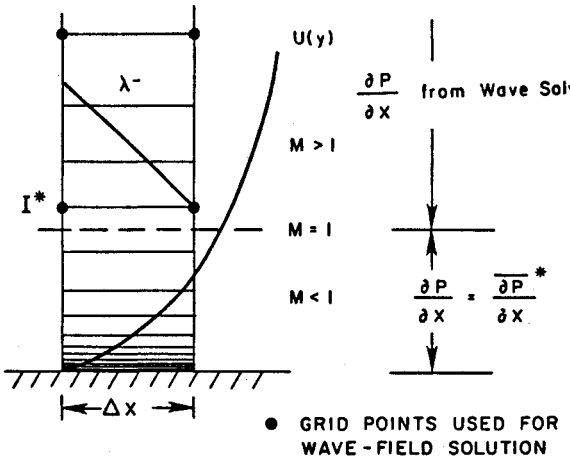

Fig. 2 Near-wall grid nomenclature and different grid scales for parabolic and hyperbolic solutions.

the procedure using compression ramp data obtained at Princeton University described in Ref. 23.

Treatment of Viscous Terms/Chemical Source Terms in Wave Solver

In the solution sequence described above, the diffusive/chemical kinetic source terms F_u, F_v, F_H, and F_{α_j} employed in the *corrected* wave-field solution correspond *exactly* to those utilized in the parabolic solution, and they are evaluated identically using the same grid network. In wall-bounded problems, where the grid is highly stretched in the near-wall region, use of the same grid network for the implicit parabolic and explicit wave-field solutions is not practical, due to the CFL step-size limitations on the wave-field solution, and the pressure is solved on a coarser scale, as exhibited in Fig. 2. In these situations, the source terms are still evaluated on the fine scale, while the coefficients associated with these terms [see Eq. (15)] are evaluated on the coarse scale, as borne out by detailed numerical studies.[16]

Inviscid Region Shock-Capturing

In most supersonic combustion problems of practical interest, the duct flow is fully turbulent, and no artificial dissipation is required to stabilize strong oblique shocks propagating through the flow. In the inviscid limit, numerical exercises (to be described) were performed to ascertain the requirements for adding artificial dissipation for shock stabilization and entropy generation to yield correct shock strengths. The use of artificial dissipation to aid shock-capturing in inviscid zones is always required in Beam and Warming central-difference-based algorithms, whereas the requirements here appear to be less stringent.

Second-order artificial dissipation is added as a run option by modifying the viscosity level ($\tilde{\mu}=\mu_l+\mu_t+\epsilon$), where the added viscosity ϵ is related to the local wave strength via the equation:

$$\epsilon=\epsilon_i\left|\frac{|\Delta P^+|-|\Delta P^-|}{|\Delta P^+|+|\Delta P^-|}\right| \tag{30}$$

where

$$\Delta P^{\pm}=P_I\pm P_{I\pm 1} \tag{31}$$

The coefficient ϵ_i utilized has values akin to those utilized in Beam and Warming[24] based codes, namely, $0<\epsilon_i<0.3$. All calculations in this article, and the original paper on which it is based, were performed with *no* artificial dissipation utilized except for the inviscid shock-capturing studies exhibited to illustrate the use of this damping option.

Numerical Studies

Comparison with SCIPPY Inviscid Shock-Capturing Solution

The pressure/wave-solver algorithm (as incorporated into the computer code entitled SPLITP) was evaluated for shock-capturing capabilities by comparing its predictions with those of the well-established SCIPPY shock-capturing model.[26] Figure 3 exhibits a typical comparison for the inviscid shock propagation pattern in a convergent duct where the incoming flow Mach number is 3. The wave-solver prediction of the pressure variation along the duct walls with no artificial viscosity added is seen to be in excellent agreement with the SCIPPY predictions. Comparisons were also made for a second case where the Mach number of the incoming flow is increased to 6. The shocks produced are now substantially stronger than those of the earlier case. As shown in Fig. 4, wave-solver calculations with no artificial dissipation added do not agree with the SCIPPY results. However, with the addition of artificial dissipation, very good agreement is obtained. The artificial dissipation parameter ϵ_i was set at 0.3 for this calculation; variations

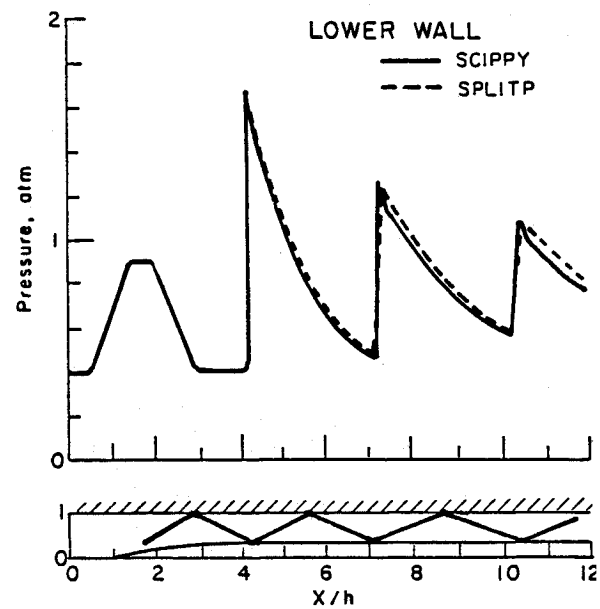

Fig. 3 Comparison of inviscid shock propagation pattern in duct for Mach 3 entrance conditions.

over the range $0.2<\epsilon_i<0.4$ produced comparable results, which did not depend strongly on the dissipation level utilized. All other calculations described in this article were performed with *no* artificial dissipation.

Comparisons with SCIPVIS PNS Shock-Capturing Solutions

In the second series of numerical studies, predictions were compared with those of the well-established SCIPVIS PNS shock-capturing model[27] for the analysis of basic interactive phenomena in supersonic mixing problems.[25,28] The most "sensitive" problem is the prediction of the perturbation waves generated by the dissipative effects of a supersonic mixing process (Fig. 5). Here, the viscous forcing function (F) terms in the wave solver generate the waves in the flow; if these viscous forcing function terms are set to zero, the pressure remains constant. Figure 6 compares perturbation pressure variations along upper and lower duct walls (treated as slip boundaries) for the mixing of Mach 2.4 and 4.8 airstreams initially at pressure of 1 atm and a temperature of 1000 K (see Ref. 28 for case description details). The two predictions are quite comparable, indicating that the pressure/viscous coupling achieved via the forcing function representation in the wave solver is compatible with the conservative "fully coupled" representation in SCIPVIS.

The next text case exhibits the interaction of a wall-generated expansion fan with the above turbulent shear layer (Fig. 6). The comparisons of the duct wall pressures are again seen to be quite favorable. In these calculations, the grid spacing used by both models was the same (41 points evenly spaced across duct, Δx given by CFL constraint), and both models employed the kW turbulence model (see Ref. 25). Further comparisons of this type (including shock/shear layer interactions) are given in Ref. 16.

Combustion-Generated Waves

To demonstrate the influence of combustion chemistry on the wave field, calculations were performed for the mixing of a Mach 2.6 H_2 stream with a Mach 2.4 airstream, initially at a pressure of 1 atm and a temperature of 1000 K. Calculations were performed with both finite-rate and frozen chemistry. The effect of H_2/air combustion on the duct pressure variation is quite pronounced, as seen by comparing the frozen and finite-rate solutions of Fig. 7. Also exhibited is the same case performed with a new version of the

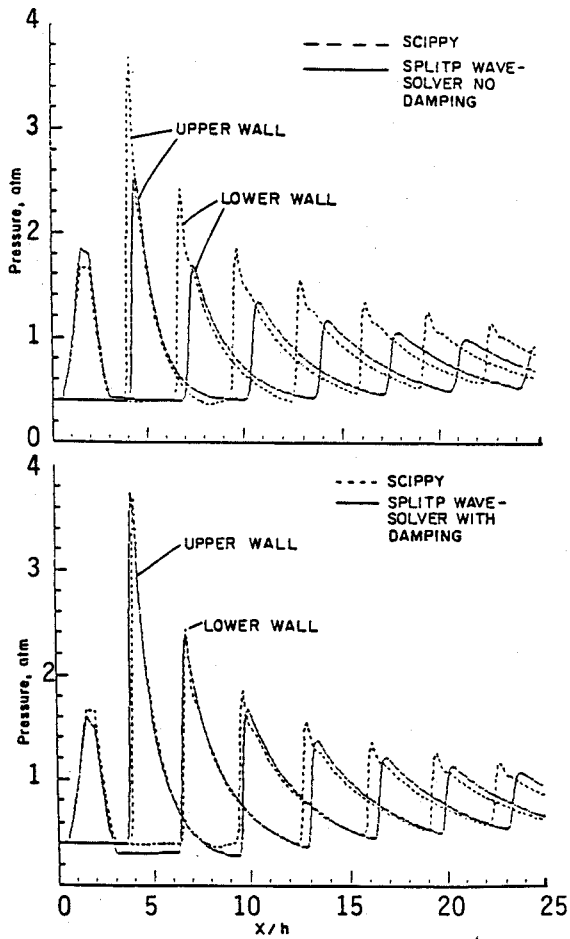

Fig. 4 Comparison of inviscid shock propagation pattern in duct for Mach 6 entrance conditions.

SCIPVIS PNS code, extended to analyze combustion chemistry.[23] The two sets of results are in reasonable agreement with further comparative studies planned to isolate numerical/grid issues for this class of problem.

Applications/Validation

Analysis of Burrows and Kurkov Experiment

Very little data are available to validate the application of the turbulent duct flow model for realistic supersonic combustion problems. The Burrows and Kurkov data[29] are among the few sets of data available that provide the detailed initial conditions required to analyze this problem properly. The case involves the sonic, tangential, balanced pressure injection of a Mach 1, cold ($T=254$ K) H_2 jet into a Mach 2.44, hot ($T=1270$ K) vitiated airstream in a near-parallel wall combustor. The airstream had a thick boundary layer, which was about three times the size of the initial H_2 jet (jet slot height was 0.4 cm). Figure 8 compares predictions (performed imposing a turbulent Prandtl number of 0.9 and utilizing the hybrid k-ϵ/Van Driest turbulence model) of H_2, N_2, O_2, and H_2O mole fractions at the combustor exit (36 cm downstream of the injection plane) with the measured data. The results are quite reasonable and accurately locate the flame position (peak H_2O) although they slightly underpredict the peak level of H_2O observed (which may require adaptive gridding that concentrates points in the flame zone). Complete details of this calculation are given in Ref. 30, which also discusses the marked sensitivity of the results on the initial profile and turbulence model initialization.

Inverse Solution/Duct Design Problem

This calculation simulates a Mach 1, cold ($T=255$ K) H_2 jet injected tangentially into a hot ($T=1270$ K), Mach 2.6

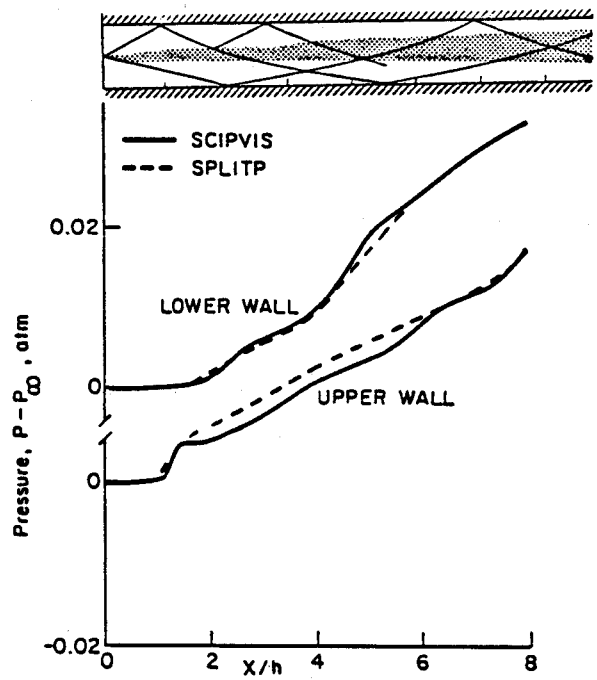

Fig. 5 Comparison of predictions for perturbation pressures generated by mixing in duct.

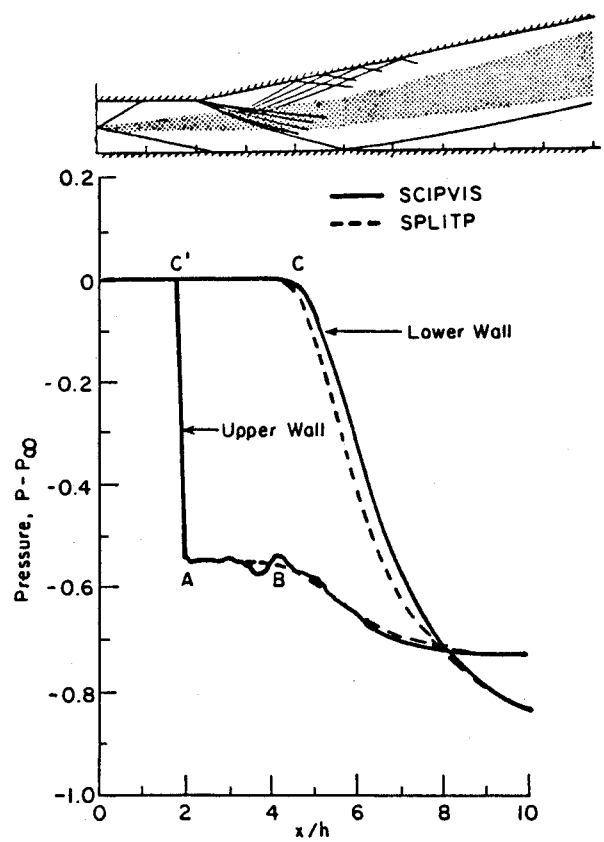

Fig. 6 Comparison of predictions of wall pressure variation for expansion fan/shear-layer interaction in diverging duct.

airstream at balanced pressure ($P=0.35$ atm). In a constant-area duct, the pressure rise generated by combustion caused the flow to separate at about 9 jet slot heights downstream of the injection plane.[34] The calculation was repeated in the inverse mode to generate combustor walls that would yield a constant pressure environment in the combustor. Figure 9 exhibits the initial injectant conditions, the predicted constant-pressure combustor geometry, and the variation of

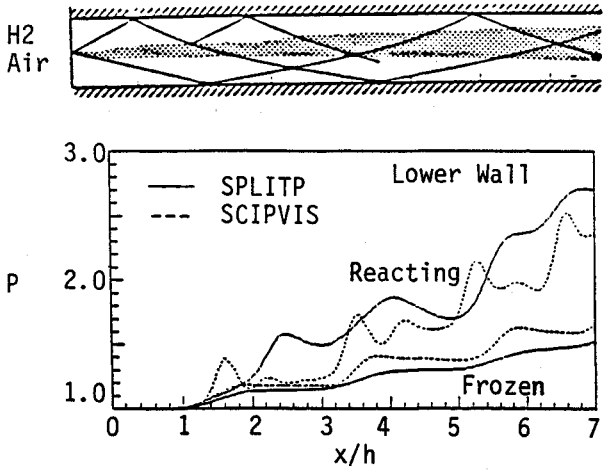

Fig. 7 Comparison of predictions for pressure rise generated by combustion in duct.

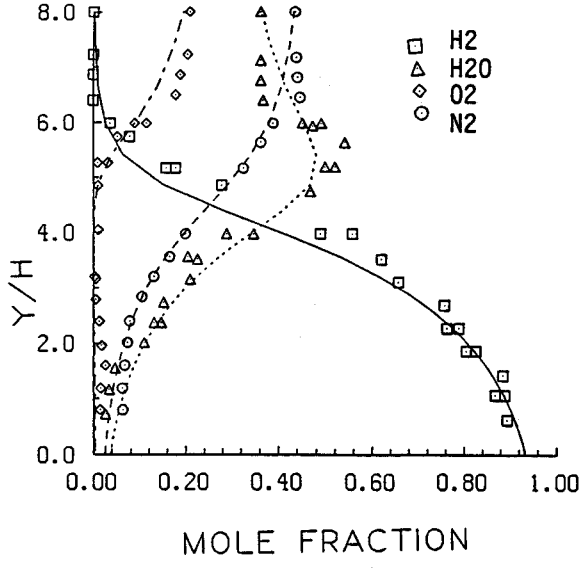

Fig. 8 Comparison of predictions with Burrows and Kurkov data for mole fraction profiles at combustor exit.

skin friction on the combustor walls. It is seen that substantial duct divergence is required in this situation to compenstate for the blockage effects of mixing and combustion.

PNS Analysis of Underexpanded Tangential Slot Injection Problem

This test case simulates the flowfield in a supersonic combustor with tangential injection at significantly higher pressure (10/1 static pressure ratio) than the surrounding airstream. The problem was performed with half-plane symmetry. Figure 10 depicts a schematic of the flow configuration, pressure contours, pressures along the wall and symmetry plane, and the variation of wall skin-friction coefficient. The skin friction is seen to respond directly to the pressure gradient along the wall with the proper dip in C_f exhibited at shock/boundary-layer interaction points, particularly noticeable for the first intersection at $x/h \sim 5$, where the shock is strong and not diffused. The ability to handle such interactions is a virtue of the near-wall coupling approach utilized,[10] whose validity is borne out by detailed comparisons with turbulent compression corner data.[23]

PNS Analysis of Underexpanded Angled Slot Injection Problem

The test case simulates the flowfield in a supersonic combustor with fuel injected at an angle of 10 deg, and also at

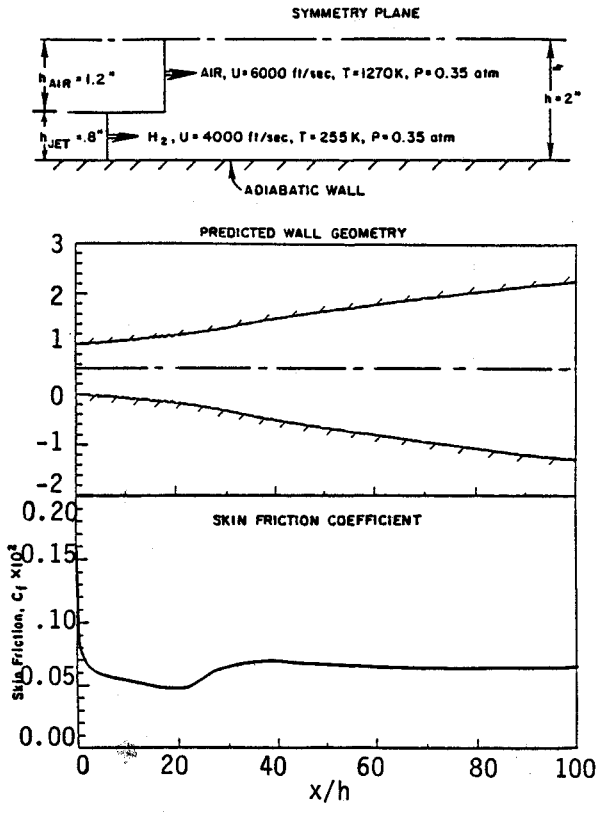

Fig. 9 Inverse design analysis of combustor: predicted wall geometry and skin friction.

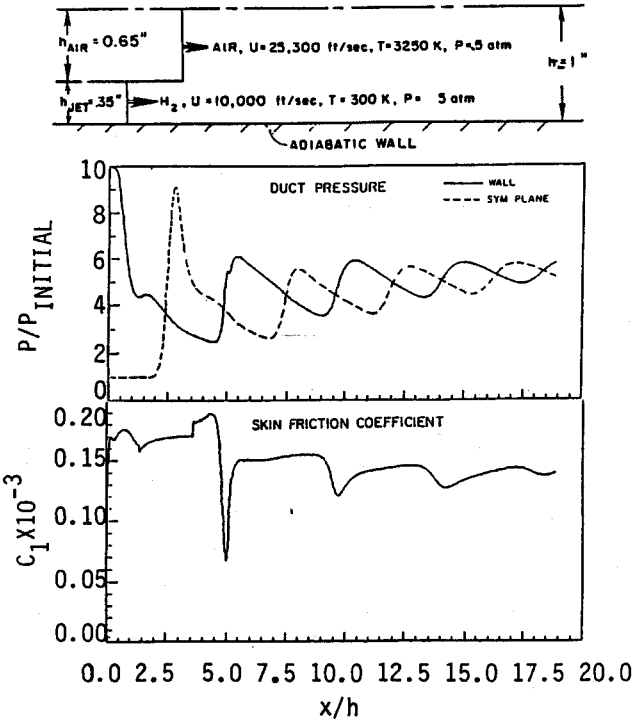

Fig. 10 Underexpanded tangential H_2 injection: combustor duct wall and centerline pressure and skin friction.

higher pressure (10/1 ratio) than the surrounding airstream. The problem was performed with half-plane symmetry. Compared to the previous fuel-rich case, this case is "almost" stoichiometric in a premixed sense. Figure 11 depicts a schematic of the flow configuration and contours of H_2O mole fractions, showing that significant combustion occurs. Unlike the previous fuel-rich case, this case is

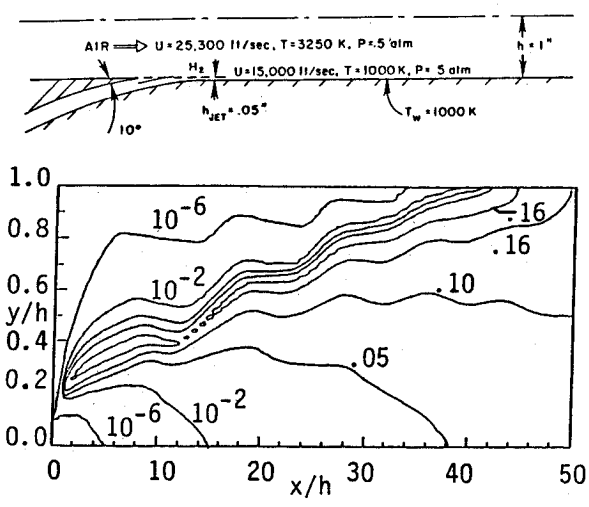

Fig. 11 Underexpanded H_2 jet, angled slot injection combustor problem: H_2O mole fraction contours.

dominated by combustion, and the waves are much weaker since the jet momentum flux is much lower.

Concluding Remarks

Features and applications of a recently developed ducted supersonic combustion model have been presented. By virtue of the splitting/decoupling techniques employed to solve distinctly the parabolic mixing, hyperbolic wave, and chemical kinetic equations, significant flexibility is available, permitting operation in Euler, parabolic (direct or inverse), and fully PNS modes, and problems with disparate mixing/wave/kinetic scales can readily be addressed. The methodology developed has been applied to a wide array of nonducted flow problems (plumes, wakes, wall jets, boundary layers) as described in Refs. 10 and 16, and has been validated for such problems utilizing a very broad data base. For scramjet supersonic combustor studies, a specialized version of this model, entitled SCORCH,[31,32] has seen widespread usage in the scramjet propulsion community, and numerous validation studies have been performed. Comparisons of these studies with available data and other code predictions should soon make their way into the open literature. The chemical kinetic and turbulence modeling utilized represents very well-established methodology, and its development in a "black box" fashion simplifies upgrades and permits transferring the capabilities to alternate models (e.g., the chemical species/kinetic and turbulence model solvers have been extracted and incorporated into a Beam-Warming-based PNS model[33]). Chemical kinetic rates/mechanisms for H_2/air combustion employ the latest established values and can readily be modified by the code user since the thermochemical data come from a generalized data base, containing reaction sets, rate data, thermodynamic data, and laminar transport data. The computer code accesses the data base through a processor to incorporate species/reactions of interest.

Acknowledgments

Principal support for the development of the numerical methodology described was provided by the NASA Langley Reasearch Center under Contract NAS1-16535. The authors are indebted to co-worker Brian York for his technical contributions to this effort.

References

[1]Ferri, A., "Review of Problems in Application of Supersonic Combustion," *Journal of the Royal Aeronautical Society*, Vol. 68, Sept. 1964, pp. 575-597.

[2]Ferri, A., "Mixing Controlled Supersonic Combustion," *Annual Review of Fluid Mechanics*, Vol. 5, Annual Reviews Inc., Palo Alto, CA, 1973, pp. 301-338.

[3]Moretti, G., "Analysis of Two-Dimensional Problems of Supersonic Combustion Controlled by Mixing," *AIAA Journal*, Vol. 3, Feb. 1965, pp. 223-229.

[4]Edelman, R. and Weilerstein, G., "A Solution of the Inviscid-Viscid Equations with Applications to Bounded and Unbounded Multicomponent Reacting Flows," AIAA Paper 69-83, Jan. 1969.

[5]Dash, S. M., "An Analysis of Internal Supersonic Flows with Diffusion, Dissipation and Hydrogen-Air Combustion," NASA CR-111783, May 1970.

[6]Dash, S. M. and DelGuidice, P. D., "Analysis of Supersonic Combustion Flowfields with Embedded Subsonic Regions," NASA CR-112223, Nov. 1972.

[7]Ferri, A. and Dash, S. M., "Viscous Flow at High Mach Numbers with Pressure Gradients," *Viscous Interaction Phenomena in Supersonic and Hypersonic Flow*, University of Dayton Press, Dayton, OH, 1970, pp. 271-318.

[8]Markatos, N. C., Spalding, D. B., and Tatchell, D. G., "Combustion of Hydrogen Injected into a Supersonic Airstream (SHIP)," NASA CR-2802, April 1977.

[9]Elghobashi, S. and Spalding, D. B., "Equilibrium Chemical Reaction of Supersonic Hydrogen-Air Jets (ALMA)," NASA CR-2725, Jan. 1979.

[10]Dash, S. M., Sinha, N., and York, B. J., "Implicit/Explicit Analysis of Interactive Phenomena in Supersonic Chemically Reacting Mixing and Boundary Layer Problems," AIAA Paper 85-1717, July 1985.

[11]Dash, S. M., Beddini, R. A., Wolf, D. E., and Sinha, N., "Viscous/Inviscid Analysis of Curved Sub- or Supersonic Wall Jets," *AIAA Journal*, Vol. 23, Jan. 1985, pp. 12-13.

[12]Mikatarian, R. R., Kau, C. J., and Pergament, H. S., "A Fast Computer Program for Nonequilibrium Rocket Predictions," Air Force Rocket Propulsion Laboratory, Edwards Air Force Base, CA, TR-72-94, Aug. 1972.

[13]Sinha, N. and Dash, S. M., "Overlaid Approach for Base Flow Analysis at Supersonic Velocities," AIAA Paper 85-1673, July 1985.

[14]Gordon, S. and McBride, B. J., "Computer Program for Calculations of Complex Equilibrium Compositions, Rocket Performance, Incident and Reflected Shocks, and Chapman-Jouguet Detonations," NASA SP-273, 1971.

[15]Svehla, R. A., "Estimated Viscosities and Thermal Conductivities of Gases at High Temperatures," NASA TR R-132, 1962.

[16]Dash, S. M. and Sinha, N., "Fully-Coupled Analysis of Jet Mixing Problems, Part II: Pressure-Split Model, SPLITP," NASA CR in preparation.

[17]Arora, R., Kuo, K. K., and Razdan, M. K., "Near-Wall Treatment for Turbulent Boundary Layer Computations," *AIAA Journal*, Nov. 1982, pp. 1481-1482.

[18]Tyson, R. J. and Kliegel, J. R., "An Implicit Integration Procedure for Chemical Kinetics," AIAA Paper 68-180, Jan. 1968.

[19]Zucrow, M. J. and Hoffman, J. D., *Gas Dynamics*, Vol. II, Wiley, New York, 1977, pp. 1-67.

[20]Anderson, D. A., Tannehill, J. C., and Pletcher, R. H., *Computational Fluid Mechanics and Heat Transfer*, McGraw-Hill, New York, 1984, pp. 247-252.

[21]Escudier, M. P., "The Distribution of Mixing Length in Turbulent Flows Near Walls," Imperial College, England, Rept. TWF/AN/1, 1966.

[22]Launder, B. E. and Spalding, D. B., *Mathematical Models of Turbulence*, Academic Press, London, 1972, p. 29.

[23]Dash, S. M., "Turbulence Modeling, Chemical Kinetic and Algorithm Related Issues in CFD Analysis of Scramjet Components," *Second National Aerospace Plane Technology Symposium*, NASP CP 2012, Vol. IV, Nov. 1986.

[24]Beam, R. W. and Warming, R. F., "An Implicit Factored Scheme for the Compressible Navier-Stokes Equations," *AIAA Journal*, Vol. 16, April 1978, pp. 393-402.

[25]Dash, S. M. and Wolf, D. E., "Iterative Phenomena in Supersonic Jet Mixing Problems, Part I: Phenomenology and Numerical Modeling Techniques," *AIAA Journal*, Vol. 22, July 1984, pp. 905-913.

[26]Dash, S. M. and Thorpe, R. D., "A Shock-Capturing Model for One and Two Phase Supersonic Exhaust Flows," *AIAA Journal*, Vol. 19, July 1981, pp. 842-851.

[27]Dash, S. M., Wolf, D. E., and Seiner, J. M., "Analysis of Turbulent Underexpanded Jets, Part 1: Parabolized Navier-Stokes Model, SCIPVIS," *AIAA Journal*, Vol. 23, April 1985, pp. 505-514.

[28]Dash, S. M. and Wolf, D. E., "Interactive Phenomena in Supersonic Jet Mixing Problems, Part II: Numerical Studies," *AIAA Journal*, Vol. 22, Oct. 1984, pp. 1395-1404.

[29]Burrows, M. C. and Kurkov, A. P., "Analytical and Experimental Study of Supersonic Combustion of Hydrogen in a Vitiated Airstream," NASA TM X-2828, Sept. 1973.

[30]Sinha, N. and Coirier, W., "Investigation of the Burrows and Kurkov Combustor Experiment with the SCORCH Computer Code," Science Applications International Corp., Princeton, NJ, SAIC/PR TM-49, Dec. 1986.

[31]Dash, S. M., Sinha, N., Wolf, D. E., and York, B. J., "Computational Models for the Analysis/Design of Hypersonic Scramjet Components—Part I: Combustor and Nozzle Models," AIAA Paper 86-1595, June 1986.

[32]Dash, S. M., "Design-Oriented PNS Analysis of Complete Scramjet Propulsive System," *Second National Aerospace Plane Technology Symposium*, NASP CP 2012, Vol. IV, Nov. 1986.

[33]Sinha, N., Krawczyk, W., and Dash, S. M., "Inclusion of Chemical Kinetics into Beam-Warming Based PNS Model for Hypersonic Propulsion Applications," AIAA Paper 87-1898, June 1987.

[34]Sinha, N. and Dash, S. M., "Parabolized Navier-Stokes Analysis of Ducted Turbulent Mixing Problems with Finite Rate Chemistry," AIAA Paper 86-0004, Jan. 1986.